

ARTICLE TYPE

Surface magnetic field of the A-type metallic-line star omicron Pegasi revisited

Yoichi Takeda

11-2 Enomachi, Naka-ku, Hiroshima-shi,
730-0851, Japan**Correspondence**

Email: ytakeda@js2.so-net.ne.jp

arXiv:2301.05367v1 [astro-ph.SR] 13 Jan 2023

The bright A-type metallic-line star *o* Peg was reported in the early 1990s to have a surface magnetic field of ~ 2 kG by analyzing the widths and strengths of spectral lines. In respect that those old studies were of rather empirical or approximate nature and the quality of observational data was not sufficient, this problem has been newly reinvestigated based on physically more rigorous simulations of line flux profiles, along with the observed equivalent widths (W) and full-widths at half-maximum (h) of 198 Fe I and 182 Fe II lines measured from the high-quality spectra. Given the Fe abundance derived from the conventional analysis, theoretical W and h values calculated for various sets of parameters were compared with the observed ones, which lead to the following conclusion regarding $\langle H \rangle$ (mean field strength). (1) An analysis of W yielded $\langle H \rangle \sim 1\text{--}1.5$ kG from Fe II lines with the microturbulence of $v_t \sim 1.5$ km s $^{-1}$. (2) A comparison of h resulted in $\langle H \rangle \sim 1.5\text{--}2$ kG as well as the projected rotational velocity of $v_e \sin i \simeq 5$ km s $^{-1}$. (3) Accordingly, the existence of mean magnetic field on the order of $\langle H \rangle \sim 1\text{--}2$ kG in *o* Peg was confirmed, which is almost consistent with the consequence of the previous work.

KEYWORDS:stars: atmospheres — stars: chemically peculiar — stars: early-type stars: individual (*o* Peg) — stars: magnetic fields**1 | INTRODUCTION**

The star *o* Peg (= HD 214994 = HR 8641 = HIP 112051; spectral type is A1 IV) is one of the most frequently studied A-type stars in stellar spectroscopy, because of its apparent brightness ($V = 4.79$) and sharp-line nature with low projected rotational velocity ($v_e \sin i \lesssim 10$ km s $^{-1}$). As is often the case with slowly-rotating stars in the upper main sequence, it is a chemically peculiar (CP) star; more specifically, because of the conspicuous overabundances in the elements heavier than the Fe group, it is regarded as a hot metallic-lined A-type (Am) star (e.g., Adelman 1988, Hill & Landstreet 1993).

Definite variability has not been confirmed, despite of the designation “Si-variable” and “variable radial velocity” in Renson & Manfroid’s (2009) catalogue of CP stars.

A remarkable and rare feature of this star is that a surface magnetic field was spectroscopically detected in the past, despite that Am stars are generally not magnetic (unlike other groups of CP stars such as the SrCrEu type).¹

— It was Mathys & Lanz (1990; hereinafter referred to as ML90) who first reported the existence of a magnetic field of $H \sim 2$ kG in *o* Peg, where they employed two independent

⁰Abbreviations: LTE, local thermodynamic equilibrium; FWHM, full width at half maximum

¹The meaning of this statement (non-magnetic nature of Am stars in general) is that appreciable magnetism (e.g., field strength on the order of \sim kG) found in magnetic CP stars is generally absent in Am stars. Recent very high-precision spectropolarimetric observations have revealed that an extremely weak magnetic field (on the order of \sim G) is detectable in several hot Am stars; Sirius (Petit et al. 2009), β UMa and θ Leo (Blazère et al. 2016a), Alhena (γ Gem) (Blazère et al. 2016b, 2020).

techniques: (i) statistical line-width analysis (Stenflo & Lindgren 1977) and (ii) empirical relation for the H -dependent difference of equivalent width (W) between Fe II 6147.7 and 6149.2 lines (which have almost the same strengths in the non-magnetic case; cf. Mathys 1990).

— Successively, numerically solving the transfer equation of polarized radiation in the presence of a magnetic field according to Takeda (1991a), Takeda (1991b; hereinafter referred to as T91b) explained the H -dependence of $W_{6147.7}/W_{6149.2}$ difference as due to the desaturation effect caused by magnetic broadening (while proposing the simultaneous use of similar line pair Fe II 4416.8/4385.4), and derived $H \sim 2\text{--}3$ kG (assuming a microturbulence of $v_t \sim 0$ km s⁻¹) for σ Peg, which is favorably compared with ML90.

— Further, Takeda (1993; hereinafter T93) devised a method for determining the magnetic field based on the W values of many lines, which is regarded as a refined version of the classical Hensberge & De Loore’s (1974) technique and can establish the (H, v_t) solution by requiring the consistency of abundances derived from lines of various strengths. Regarding σ Peg, T93 concluded $H \sim 2$ kG (and $v_t \sim 1.5$ km s⁻¹), which is again consistent with ML90.

Since then, however, little progress seems to have been made as to the corroboration of these findings. As already noted by ML90, the spectropolarimetric technique (most commonly used for investigating magnetic fields of CP stars) has been unsuccessful to accomplish a meaningful detection in σ Peg (though extremely weak magnetic field might as well be still detectable as remarked in footnote 1). Actually, besides the pioneering work of Babcock (1958), Shorlin et al. (2002) could not detect any $\langle H_z \rangle$ (disk-averaged line-of-sight component of the field) of significance in σ Peg by their spectropolarimetric observation coupled with Least-Squares-Decomposition (LSD) technique.²

This suggests that $\langle H_z \rangle$ happens to be too small (presumably because components of opposite signs are cancelled out by disk integration) to produce a significant signal of circular polarization.

Accordingly, in order to study the magnetic nature of σ Peg, the best way would be to analyze the equivalent widths or line widths of many spectral lines (which contain information of “absolute” magnetic field strengths) as previously done. However, it may be premature to regard the results of those old studies as sufficiently reliable because several problems are involved from a methodological point of view.

- The analysis of ML90 was not based on a rigorous modeling but a rather tentatively postulated analytical relation between the line width, line strength, and Zeeman-broadening parameters. Especially, since the original Stenflo & Lindgren’s (1977) work (on which their study is based) was intended to estimate the solar magnetic field at the disk center, the effect of rotational broadening on the line width was not taken into account; thus, how the stellar projected rotational velocity ($v_e \sin i$) affects the functional form of the relation is unclear.
- Although T91b simulated the emergent profiles and the strengths of spectral line pairs by correctly treating the transport of polarized radiation in a magnetic field, only the specific intensity profiles at the disk center ($\mu = \cos \theta = 1$) were calculated for several single-valued field strengths (H) and different angles between the magnetic field vector and the line of sight (ψ), which must be unrealistic for comparing with the flux profiles of magnetic stars. Another problem is the choice of microturbulence: $v_t \sim 0$ km s⁻¹ adopted in T91b is not consistent with that obtained later by T93 (~ 1.5 km s⁻¹); if the latter were chosen, a considerably higher magnetic field ($\sim 4\text{--}5$ kG) would have resulted (cf. Sect. 4.1 in T91b).
- The results of T93 were actually not robust but rather delicate, because H could be firmly established only from Fe II lines among the three species (finding a definite solution was difficult for Fe I and Ti II lines). Above all, the validity of the approximate method for evaluating the flux equivalent width under a magnetic field proposed by T93 (denoted as W_b , which is a simple mean between the minimum and maximum intensification cases) should be quantitatively checked in the first place.
- Attention should also be paid to the adopted observational data of σ Peg. ML90’s measurements of line widths for their application of Stenflo–Lindgren technique were done on spectra with a signal-to-noise ratio (S/N) of ~ 100 covering 3700–4650 Å resulting from the co-added photographic spectrogram with a reciprocal dispersion of 2.4 Å mm⁻¹ obtained at Dominion Astrophysical Observatory (Adelman, Cowley, & Hill 1988). Similarly, the equivalent width data of Fe I, Fe II, and Ti II lines for σ Peg adopted in the analysis of T93 were taken from Adelman’s (1988) Table 5, for which he used the same co-added Dominion spectra. Since the quality of these photographic spectra is not sufficient from the viewpoint of present-day standard and using only the blue-region data is not advantageous for the purpose of magnetic-field detection, it is desirable to employ modern spectra of much higher quality covering wider (from blue through red) wavelength range.

²According to the compilation of Bychkov, Bychkova, & Madej (2009), σ Peg’s $\langle H_z \rangle$ resulting from Shorlin et al.’s (2002) observation was $32(\pm 20)$ G, which would have been regarded as under the level of significance.

As such, it is worth reinvestigating the magnetic field of *o* Peg by analyzing the widths and strengths for a number of spectral lines as done by ML90 and T93 but based on physically rigorous theoretical line-profile modeling along with new observational data. Given this situation and now that CCD spectra of very high S/N for this star are now available, I decided to freshly revisit this problem, while making use of the profile simulation program based on disk integration coupled with the solution code of polarized radiation transfer in a magnetic field. The purpose of this paper is to report the results of this new analysis.

2 | OBSERVATIONAL DATA

2.1 | Observed spectra of *o* Peg

The high-dispersion spectra of *o* Peg adopted in this investigation are the same as used in Takeda et al.’s (2012) abundance study of alkali elements for A-type stars. The observations were done on UT 2008 October 4 (8 frames of 1200 s exposure within a time span of ~ 6 hr), October 7 (1 frame of 1800 s exposure), October 8 (8 frames of 1200 s exposure within a time span of ~ 3 hr), and October 9 (6 frames of 1200 s exposure within a time span of ~ 2 hr) by using the HIDES (High Dispersion Echelle Spectrograph) placed at the coude focus of the 1.88 m reflector at Okayama Astrophysical Observatory. Equipped with three mosaicked 4K \times 2K CCD detectors at the camera focus, echelle spectra covering 4100–7800 Å (in the mode of red cross-disperser) with a resolving power of $R \sim 100000$ (corresponding to the slit width of 100 μm) were obtained.

The reduction of the spectra (bias subtraction, flat-fielding, scattered-light subtraction, spectrum extraction, wavelength calibration, and continuum normalization) was performed by using the “echelle” package of the software IRAF³ in a standard manner. In order to improve the signal-to-ratio, all available frames were co-added, by which very high S/N (typically around ~ 1000 on the average) could be accomplished in the final spectra as shown in Fig. 1 ($S/N \sim \sqrt{\text{count}}$).

2.2 | Selected lines and measurements

In this study, we concentrate to using only spectral lines of Fe I and Fe II, as they are available in larger number over a wide range of strengths than other species. The candidate lines to be analyzed were carefully sorted out by inspecting the observed spectral feature while comparing it with the calculated strengths of neighboring lines as well as the synthesized

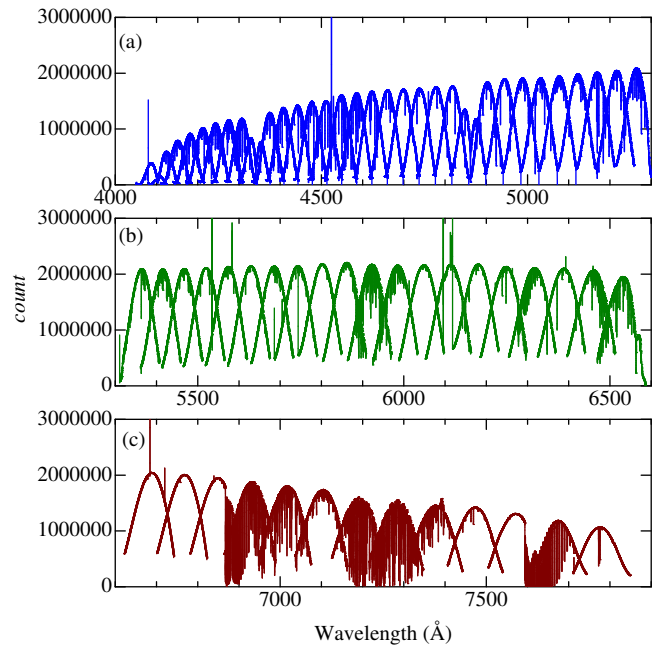


FIGURE 1 Panels (a), (b), and (c) show the distributions of accumulated photoelectron counts of CCD for the final spectra of *o* Peg, each corresponding to three wavelength regions (4100–5300/5300–6600/6600–7900 Å) comprising 32/20/13 orders, respectively. Note that the signal-to-noise ratio can be estimated as $S/N \sim \sqrt{\text{count}}$ in the present photon-noise-limited case. The spectra in each of the echelle orders show characteristic distributions of the blaze function.

theoretical spectrum, as done by Takeda (2020). Because of the necessity of calculating the Zeeman components, those lines lacking the information of quantum numbers (L , S , J) for the lower and upper levels were excluded. As a result, 198 Fe I and 182 Fe II lines were selected. The equivalent widths (W_λ) of these lines were measured by fitting the line-depth profile ($R_\lambda \equiv 1 - f_\lambda/f_{\text{cont}}$) with the Gaussian function ($\propto \exp[-(\lambda - \lambda_0)^2/a^2]$), while the line widths (h_λ ; defined as the FWHM of R_λ) were directly evaluated from the profiles.

The W_λ values of these Fe lines range from ~ 1 mÅ to ~ 200 mÅ (Fig. 2a) and their effective Landé factors are between $0 \lesssim g_{\text{eff}}^L \lesssim 3$ (Fig. 2b). As seen from the empirical curves of growth depicted in Fig. 2c, the linear part and the shoulder/flat part are roughly separated around $10^6 W_\lambda/\lambda \sim 10$ (typically several tens mÅ in W_λ). A comparison of the equivalent widths with those published by Adelman (1988) is displayed in Fig. 2d, where a reasonable consistency is observed. Fig. 2e shows that the directly measured FWHM values (h_λ) are mostly in agreement with the corresponding Gaussian-fit ones (derived from the e -folding half-width as $h_\lambda^{\text{G.F.}} \equiv 2\sqrt{\ln 2} a$). The dependence of h_ν (in the velocity unit

³IRAF is distributed by the National Optical Astronomy Observatories, which is operated by the Association of Universities for Research in Astronomy, Inc. under cooperative agreement with the National Science Foundation.

derived as $h_\lambda c/\lambda$: c is the speed of light) upon the equivalent width is illustrated in Fig. 2f, which shows that h_ν begins to exhibit a systematic W_λ -dependence at $10^6 W_\lambda/\lambda \gtrsim 10$.

The measured W and h values of these 380 Fe lines along with their atomic data (wavelength, excitation potential, oscillator strengths, damping constants, term information, effective Landé factor, etc.) mostly taken from the VALD database (Ryabchikova et al. 2015) are summarized in “felines.dat” of the online material, where the original profile data of all lines are also given in “obsprofiles.dat”.

3 | CONVENTIONAL ANALYSIS OF EQUIVALENT WIDTHS FOR MICROTURBULENCE

Before dealing with the main issue of magnetic field estimation to be described in Sect. 4 and 5, we first conduct a preparatory analysis of determining the microturbulence based on the equivalent widths by applying the conventional procedure (while assuming as if no magnetic field exists).

3.1 | Atmospheric model and parameters

Regarding the standard model atmosphere of σ Peg, we adopted Kurucz’s (1993) ATLAS9 solar abundance model with $T_{\text{eff}} = 9500$ K, $\log g = 3.60$ (cgs unit). These atmospheric parameters were chosen by inspecting the various literature data summarized in Table 1. As recognized from this table, these values (though rather rounded) are consistent with those derived in many of the past studies (especially the recent ones published after 2000). Besides, this choice is in accord with $M = 2.8M_\odot$ (mass) and $R = 4.4R_\odot$ (radius) evaluated from the position on the $\log L$ (luminosity) vs. T_{eff} diagram in comparison with theoretical evolutionary tracks (see, e.g., Fig. 1 in Takeda et al. 2012). Abundance determination from an equivalent width for a given microturbulence was done by using Kurucz’s (1993) WIDTH9 program while assuming LTE. The adopted line parameters are given in “felines.dat” (see Sect. 2.2).

Two approaches are tried in this v_t determination test; (1) usual method of finding the minimum abundance dispersion, and (2) alternative method requiring the overall consistency between the observed and theoretical W .

3.2 | Method 1: minimum abundance dispersion

The effect of v_t on abundance determination appreciably depends on line strengths: abundances determined from weak lines in the linear part of the curve of growth are essentially free

from v_t , while those from stronger lines on the shoulder-to-flat part are considerably v_t -dependent. Therefore, v_t is usually established by requiring that abundances derived from lines of various equivalent widths (W) be consistent with each other.

Among the several practical procedures for accomplishing this requirement, Blackwell et al.’s (1976) method is used here.

–(1) For each line n , a set of abundances (A_n^k ; $k = 1, 2, \dots, K$) are derived from W_n while incrementally changing the microturbulence (v_t^k ; $k = 1, 2, \dots, K$).

–(2) Then, the mean abundance ($\langle A \rangle^k$) averaged over N lines and the standard deviation σ_A^k are calculated for each of the K microturbulences (v_t^k).

–(3) By inspecting the resulting standard deviation (σ_A^k ; $k = 1, 2, \dots, K$), the location of minimum σ_A corresponds to desired solution of v_t .

This procedure was applied to our data set of Fe lines. The resulting A vs. v_t relations for each of the lines along with the corresponding σ_A vs. v_t curve are shown in Figs. 3a and 3b for Fe I ($N_1 = 198$) and Fe II lines ($N_2 = 182$), respectively. As seen from these figures, we obtain $(1.71 \text{ km s}^{-1}, 7.75)^4$ and $(1.76 \text{ km s}^{-1}, 7.82)$ as the results of $(v_t, \langle A \rangle)$ for Fe I and Fe II; and the corresponding A_n for each line is plotted against W_n in Figs. 3c and 3d, respectively.

3.3 | Method 2: minimum equivalent width dispersion

Next, another method for v_t determination is tried. Since $A = 7.8$ may be regarded as the fiducial Fe abundance of σ Peg from the results of 7.75 (Fe I) and 7.82 (Fe II) derived in the previous subsection, we can calculate the theoretical equivalent widths ($W_{\text{cal},n}^{k,7.8}$; $n = 1, 2, \dots, N$) for each of the lines with this fixed Fe abundance but incrementally changing v_t^k , which are to be compared with the observed ones ($W_{\text{obs},n}$; $n = 1, 2, \dots, N$). Then, by examining the standard deviations σ_W^k evaluated for various v_t^k values,

$$\sigma_W^k \equiv \sqrt{\sum_{n=1}^N (W_{\text{cal},n}^{k,7.8} - W_{\text{obs},n})^2 / N}, \quad (1)$$

we can find the solution of v_t as that accomplishing the minimum σ_W^k . Although the final W_{cal} calculated with such determined v_t is not exactly equal to the observed W_{obs} (because of the fixed Fe abundance), the primary aim of line-independent consistency (i.e., without any global W -dependent trend) can be accomplished.

The differences $W_{\text{cal},n}^{k,7.8} - W_{\text{obs},n}$ for each lines are plotted against v_t in Fig. 4a (Fe I) and 4b (Fe II), where the corresponding σ_W versus v_t curves are also depicted. From these figures,

⁴ A is the logarithmic number abundance of Fe relative to H, which is expressed in the usual normalization of $\log[N(\text{Fe})/N(\text{H})] + 12$.

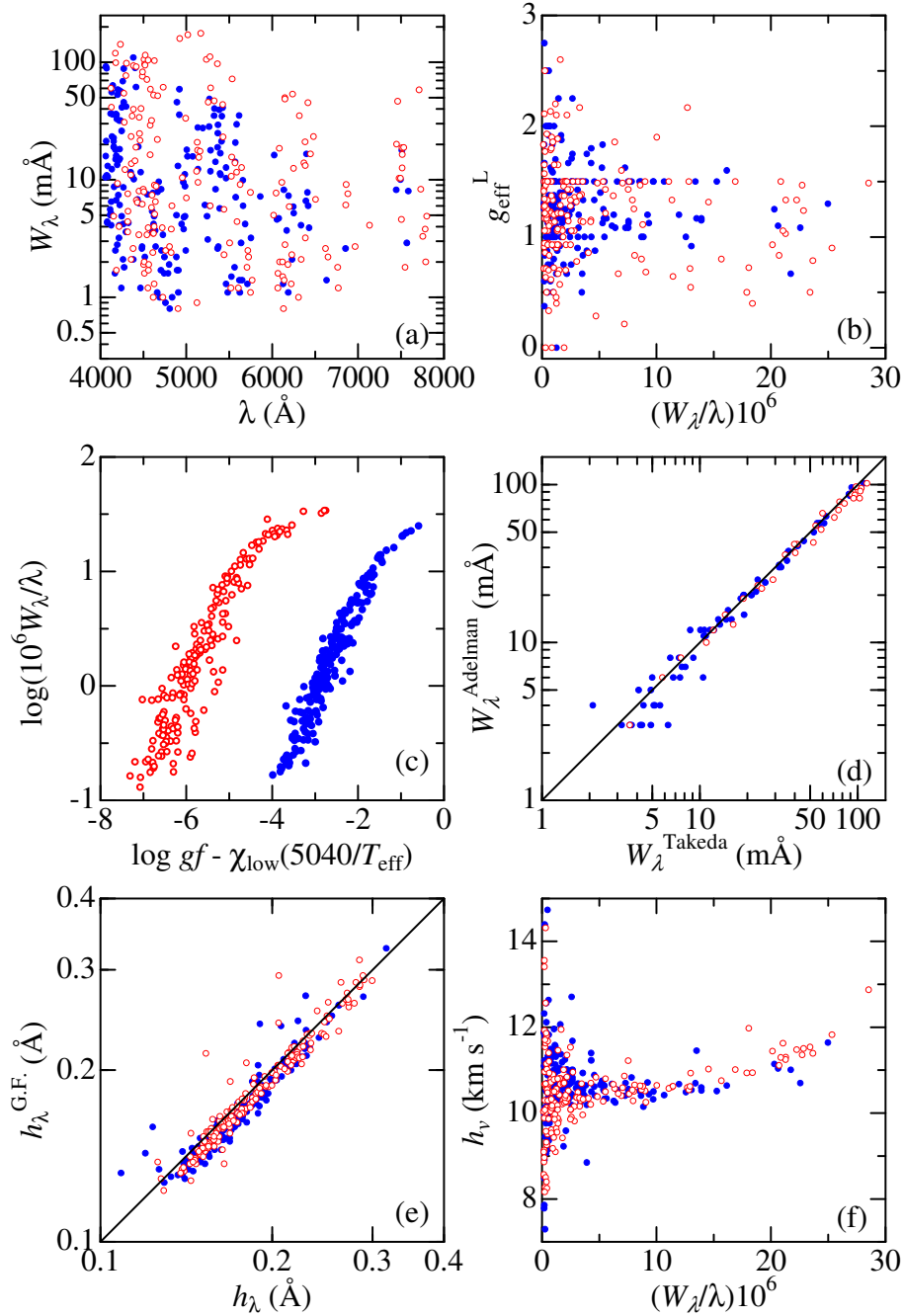


FIGURE 2 (a) Equivalent width vs. wavelength. (b) Effective Landé g factor vs. reduced equivalent width. (c) Empirical curves of growth for the Fe I and Fe II lines, where $\log gf - \chi_{\text{low}}(5040/T_{\text{eff}})$ is taken in the abscissa (g : statistical weight of the lower level, f : oscillator strength, χ_{low} : lower excitation potential in eV, T_{eff} : effective temperature in K). (d) Comparison of the equivalent widths measured in this study with those published by Adelman (1988) for 97 lines (65 Fe I lines and 32 Fe II lines) in common. (e) Correlation between the directly measured full-widths at half-maximum (h_λ) with the corresponding Gaussian-fit values ($h_\lambda^{\text{G.F.}}$). (f) Full-widths at half-maximum in the velocity unit ($h_\nu \equiv ch_\lambda/\lambda$; c is the speed of light) plotted against the reduced equivalent widths. In each panel, the data for Fe I and Fe II lines are discriminated in blue filled symbols and red open symbols, respectively.

we obtain 1.38 km s^{-1} and 1.77 km s^{-1} for Fe I and Fe II,

respectively. The differences $W_{\text{cal},n}^{k,7.8} - W_{\text{obs},n}$ for each lines corresponding to these v_t solutions are plotted against $W_{\text{obs},n}$ in Fig. 4c (Fe I) and 4d (Fe II),

TABLE 1 Atmospheric parameters of *o* Peg published so far.

Authors	T_{eff}	$\log g$	v_t	[Fe/H]	$v_e \sin i$
Wolff (1967)	9330	3.2	2.0	0.30	
Conti & Strom (1968)	9500	4.0	3.0	0.2 ^a	
Adelman (1973)	10100	4.0	3.0	0.1	
Allen (1977)	9600	3.8	3.2	-0.09	
Mitton (1977)	9500	3.5	1.6	0.08 ^b	
Adelman et al. (1984)	9625	3.45	1.6	0.20	
Adelman & Fuhr (1985)			1.9	0.26	
Adelman (1988)	9600	3.60	1.3	0.10	6
Castelli & Hack (1988)	9590	3.55	1.9	0.14	6
Kocer et al. (1988)	9500	3.50	1.5	0.04	
Sadakane (1988)	9500	3.50	2.0	0.02	
Van't Veer et al. (1988)	9350	3.50	1.5	0.02	
Burkhart & Coupry (1991)	9650	3.6		0.1	
Hill & Landstreet (1993)	9680	3.71	1.5 ^c	0.03	
Abt & Morrell (1995)					10
Hill (1995)			1.7	0.19	6.3
Sokolov (1995)	10050				
Blackwell & Lynas-Gray (1998)	9443				
Di Benedetto (1998)	9720				
Hui-Bon-Hoa (2000)	9650	3.6	1.5	0.42	≤ 10
Adelman et al. (2002)	9591	3.64			
Adelman et al. (2002)	9525	3.70			
Royer et al. (2002)					14
Royer et al. (2007)					14
Landstreet et al. (2009)	9500	3.62	2.0	0.14 ^d	7
Zorec et al. (2009)	9930				
Prugniel et al. (2011)	9373	3.73		-0.14	
Takeda et al. (2012)	9453	3.64	3.1	0.13 ^e	6.0
Zorec & Royer (2012)	9506	3.73 ^f			14
Gray (2014)	9600	3.7		0.0 ^g	6.00 ^h
Takeda et al. (2018)	9453	3.64	2.7	0.18 ⁱ	6.6

Summarized here are the effective temperature (in K), logarithmic surface gravity in c.g.s unit (in dex), microturbulence (in km s^{-1}), Fe abundance relative to the Sun, and projected rotational velocity (in km s^{-1}) of *o* Peg taken from previous publications. Since these parameters were determined in variously different methods, the original references should be consulted for the details. Regarding [Fe/H], if only those derived from Fe I and Fe II lines are available, a simply averaged value of these two is listed here. Besides, in case that the reference solar Fe abundance is not explicitly given, an appropriate value widely used at the time of publication was tentatively adopted.

^aRelative to the mean of 4 standard stars.

^bRelative to Procyon.

^cAssumed.

^dSolar Fe abundance of $\log(\text{Fe}/\text{H})_{\odot} = -4.49$ was assumed.

^eSolar Fe abundance of $A_{\odot}(\text{Fe}) = 7.50$ was assumed.

^fDerived from L (bolometric luminosity), T_{eff} , and M (mass).

^gAssumed.

^hRadial-tangential macroturbulence of $\zeta_{\text{RT}} = 5.7 \text{ km s}^{-1}$ was adopted.

ⁱRelative to Procyon.

A comparison of v_t (Method 1) derived in Sect. 3.2 with this v_t (Method 2) suggests that, while we can confirm a good agreement for the case of Fe II lines ($1.76/1.77 \text{ km s}^{-1}$), a discrepancy is seen for v_t based on Fe I lines ($1.71/1.38 \text{ km s}^{-1}$). As a matter of fact, the results from Fe I lines appear to be somewhat problematic. As can be seen in Fig. 3c, the distribution of $W_{\text{cal},n}^{k,7.8} - W_{\text{obs},n}$ differences for Fe I lines of medium-to-large strengths ($W_{\text{obs}} \gtrsim 10 \text{ m}\text{\AA}$) shows some asymmetric feature (i.e., positive for lines of 20–50 $\text{m}\text{\AA}$ while negative for those of $\gtrsim 50 \text{ m}\text{\AA}$). This trend has made the σ_W^k curve shallower with a less clear minimum (Fig. 4a), which eventually leads to larger uncertainties in v_t determination. Generally speaking, since only a very tiny fraction of Fe atoms remain

neutral (those in Fe II and Fe III stages are dominant) in the atmosphere of A-type stars, the formation of Fe I lines is considerably T -dependent and vulnerable to model atmosphere structure, while Fe II lines are more robust in this respect (see Appendix A2 of Takeda 2020). Accordingly, Fe II lines may yield more reliable results than Fe I lines.

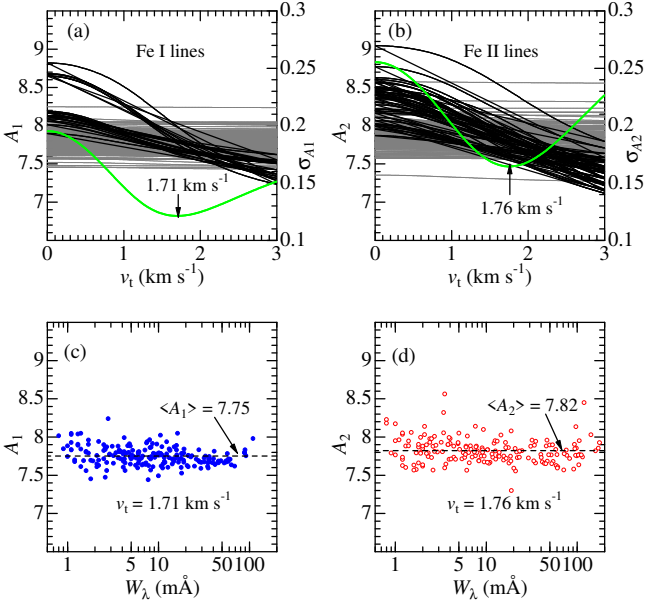


FIGURE 3 Upper panels (a), (b): solid lines show how the Fe abundance (A) of each line varies by changing v_t , where weaker lines ($10^6 W_\lambda/\lambda < 10$) and stronger lines ($10^6 W_\lambda/\lambda > 10$), are distinguished by gray and black lines, respectively. In addition, σ_A (standard deviation of A) is plotted against v_t by the thick green solid line (its scale is marked in the right axis), and the v_t solution corresponding to the minimum σ_A is also indicated. Lower panels (c), (d): Fe abundances corresponding to the v_t solution are plotted against the observed equivalent widths. The mean abundance ($\langle A \rangle$) is also indicated by the horizontal dashed line. The left-hand and right-hand panels are for Fe I and Fe II lines, respectively.

4 | LINE PROFILE SIMULATION OF A MAGNETIC STAR

4.1 | Magnetic field model

As already mentioned in Sect. 1, the main aim of this investigation is to check the previously reported results (possible existence of a magnetic field on the order of ~ 2 kG in α Peg) based on physically legitimate simulations of Zeeman-broadened line profiles. What matters here is the choice of rotating magnetic star models (field configuration, inclination of magnetic/rotational axes viewed by an observer, etc.) among diversified possibilities. In the context of lacking information, we tentatively assume a model which is as simple as possible but does not yield results contradicting the known observational facts. In any case, given that we are primarily interested in the value of $\langle H \rangle$ (mean field strength averaged over the disk; cf. Eq. (3)), we do not need to be too much particular

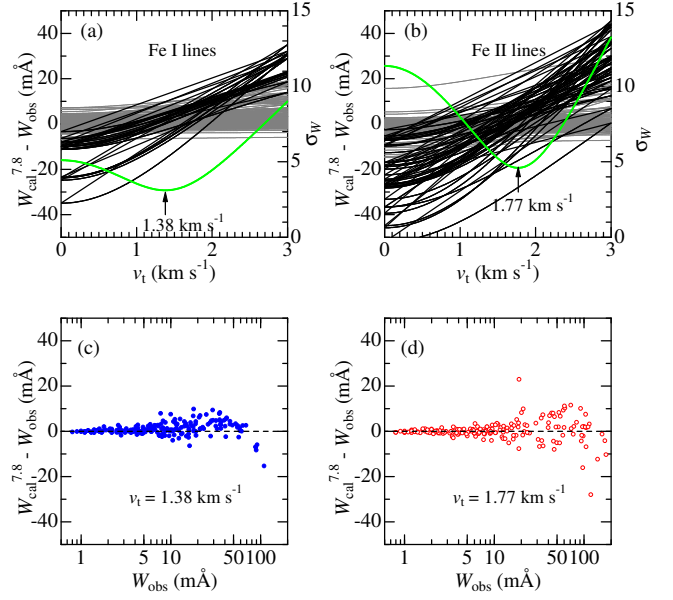


FIGURE 4 Upper panels (a), (b): solid lines show how the difference between the theoretical equivalent width calculated for $A = 7.8$ ($W_{\text{cal}}^{7.8}$) and the observed equivalent width (W_{obs}) varies by changing v_t , where weaker and stronger lines are distinguished by gray and black lines, respectively (as in Fig. 3). The standard deviation (σ_W) of the differences defined by Eq. (1) is depicted against v_t in thick green line (scale is in the right axis). Lower panels (c), (d): Equivalent width differences ($W_{\text{cal}}^{7.8} - W_{\text{obs}}$) corresponding to the v_t value of minimum σ_W are plotted against W_{obs} . The left-hand and right-hand panels are for Fe I and Fe II lines, respectively.

about this issue, because the functionality of $h(\langle H \rangle, v_e \sin i)$ or $W(\langle H \rangle, v_t)$ would not be very sensitive to any choice of models in the first approximation,

Following this policy, a simple dipole model is adopted in this study, which is represented in the spherical coordinate system as follows:

$$\begin{aligned} H_r &= H_{\text{pol}}(R/r)^3 \cos \theta \\ H_\theta &= (H_{\text{pol}}/2)(R/r)^3 \sin \theta \\ H_\phi &= 0, \end{aligned} \quad (2)$$

where H_{pol} is the magnetic field strength at the magnetic pole on the stellar surface ($r = R$, $\theta = 0^\circ$), which yields $(H_r, H_\theta, H_\phi) = (H_{\text{pol}} \cos \theta, H_{\text{pol}}/2 \sin \theta, 0)$ at the stellar surface ($r = R$). Accordingly, the absolute strength of the surface field is largest at the magnetic pole ($\theta = 0^\circ$, $|\mathbf{H}| = H_{\text{pol}}$) and smallest at the equator ($\theta = 90^\circ$, $|\mathbf{H}| = H_{\text{pol}}/2$)

As to the axis orientation and view angle of this model star, we assume that the magnetic and rotational axes are in line with each other and perpendicular to the observer's line of sight;

i.e., $i = \alpha = 90^\circ$ (as usual, i and α are the angles of rotational and magnetic axes in reference to the line of sight), as shown in the upper illustration of Fig. 5. This simple assumption is reasonable in context of the observational characteristics of α Peg, because (i) the magnetic field configuration viewed by the observer does not depend upon the rotational phase (i.e., no appreciable variability) and (ii) the line-of-sight component of the field is cancelled out by averaging over the disk to result in $\langle H_z \rangle = 0$ (meaningful circular polarization signal is undetected). The observed aspect of surface magnetic field in this model is schematically depicted in the lower-left panel (meridional cross section) and lower-middle panel (observer's view) of Fig. 5. Besides, the magnetic field strengths $|\mathbf{H}|$ (in unit of H_{pol}) at various points on the visible disk are plotted against $\cos \psi$ (ψ is the angle between the field vector and the line of sight) in the lower-right panel of Fig. 5, from which we can see that $|\mathbf{H}|$ is between $H_{\text{pol}}/2$ and H_{pol} .

4.2 | Calculation of local I profiles

As to the calculation of specific intensity profile (I_λ) of a line under the presence of a magnetic field, Unno's (1956) radiative transfer equation in terms of the Stokes parameters (I, Q, V) was solved with the help of Takeda's (1991a) numerical procedure (cf. Sect. 2 therein) as done by T91b. The line opacity profiles of Zeeman-split π , σ_+ , and σ_- components (derived from S , L , and J of upper and lower levels by assuming LS coupling) for a given magnetic field were evaluated by making use of the line opacity data of non-magnetic case calculated by the WIDTH9 program (with the same model atmosphere as adopted in Sect. 3). The necessary parameters for computing the I_λ profile emergent from a disk point are $|\mathbf{H}|$, ψ , μ (direction cosine of the angle between the surface normal and the line of sight), along with A (Fe abundance) and v_t (microturbulence). Accordingly, a grid of emergent I_λ^{grid} profiles (up to 1\AA from the line center with a step of 0.005\AA) were computed in advance for each of the 380 lines for combinations of 31 $|\mathbf{H}|$ values (0, 200, 400, ..., 5800, 6000 G), 10 ψ values (0, 10, 20, ..., 80, 90°), 10 μ values (0.1, 0.2, 0.3, ..., 0.9, 1.0), and 7 v_t values (0.0, 0.5, 1.0, ..., 2.5, 3.0 km^{-1}), while the Fe abundance was fixed at $A = 7.80$ (cf. Sect. 3).

4.3 | Line flux profile by disk integration

The flux profile F_λ of a spectral line can then be simulated by integrating the I_λ at each point of the visible disk (evaluated by interpolating the grid of I_λ^{grid} corresponding to the local physical condition), while adequately taking into account the Doppler shift due to the line-of-sight velocity. For this purpose, we modified the program CALSPEC (Takeda, Kawanomoto, & Ohishi 2008) which simulates the spectral line profile of a

rotating star by dividing its surface into 180×360 segments. Since only the case of slow rotation is considered, the effects of gravity darkening and gravitational distortion were neglected; therefore, the star is spherical and homogeneously covered with the solar abundance atmosphere of $T_{\text{eff}} = 9500$ K and $\log g = 3.60$. The parameters of H_{pol} and $v_e \sin i (= v_e)$ have to be assigned (along with v_t and A) in this modeling of line flux profile.

The calculations of F_λ for each line were done for 13 H_{pol} values (0, 500, 1000, ..., 5500, 6000 G), 7 $v_e \sin i$ values (0.0, 2.5, 5.0, ..., 12.5, 15.0 km s^{-1}), and 7 v_t values (0.0, 0.5, 1.0, ..., 2.5, 3.0 km^{-1}), again at the fixed $A = 7.80$. Further, the equivalent widths (W_{cal}) and FWHMs (h_{cal}) were also evaluated from these line profiles. As an example of simulation, the F_λ results derived for representative three lines (Fe I 4383.544, Fe II 6147.734, and Fe II 6149.246) are displayed in Fig. 6, where the corresponding observed profiles are also shown for comparison.

For the sake of future discussion, the mean absolute field strength averaged over the visible stellar disk ($\langle H \rangle$) is defined as follows:

$$\langle H \rangle \equiv \frac{\iint_{\text{disk}} |\mathbf{H}|(x, y) I_{\text{cont}}(x, y) dx dy}{\iint_{\text{disk}} I_{\text{cont}}(x, y) dx dy}, \quad (3)$$

where $|\mathbf{H}|(x, y)$ and $I_{\text{cont}}(x, y)$ are the absolute field strength and the continuum specific intensity (to the observer) at the disk point (x, y) , respectively. Naturally, $\langle H \rangle$ is in proportion to H_{pol} with the proportionality constant of $\langle H \rangle / H_{\text{pol}} = 0.642$ in the postulated magnetic field configuration ($\alpha = 90^\circ$). Likewise, the disk-averaged line-of-sight component (in the z -direction) of the magnetic field ($\langle H_z \rangle$) is definable in the similar manner and $\langle H_z \rangle = 0$ holds in the present case.

5 | MAGNETIC FIELD DETERMINATION

5.1 | Equivalent widths analysis

Let us first try to establish (H_{pol}, v_t) from equivalent widths (W). Here, Method 2 described in Sect. 3.3 is applied, in which $W_{\text{cal}}^{7.8}$ (theoretical equivalent width calculated with $A = 7.8$)⁵ is compared with W_{obs} . Since theoretical $W_{\text{cal}}^{7.8}$ data are prepared for combinations of H_{pol} and v_t (while results for $v_e \sin i = 0$ were adopted because of its irrelevance in this case), σ_W defined by Eq. (1) is also regarded as a function of these two parameters.

⁵The integrated strengths (equivalent widths) of unsaturated weak lines in the linear part of the curve of growth, which essentially determine the abundance, are practically free from any Zeeman broadening effect (like the effect of microturbulence). Accordingly, the Fe abundance of $A = 7.8$ derived in Sect. 3.2 by the conventional analysis is invariably valid irrespective of the existence of any magnetic field.

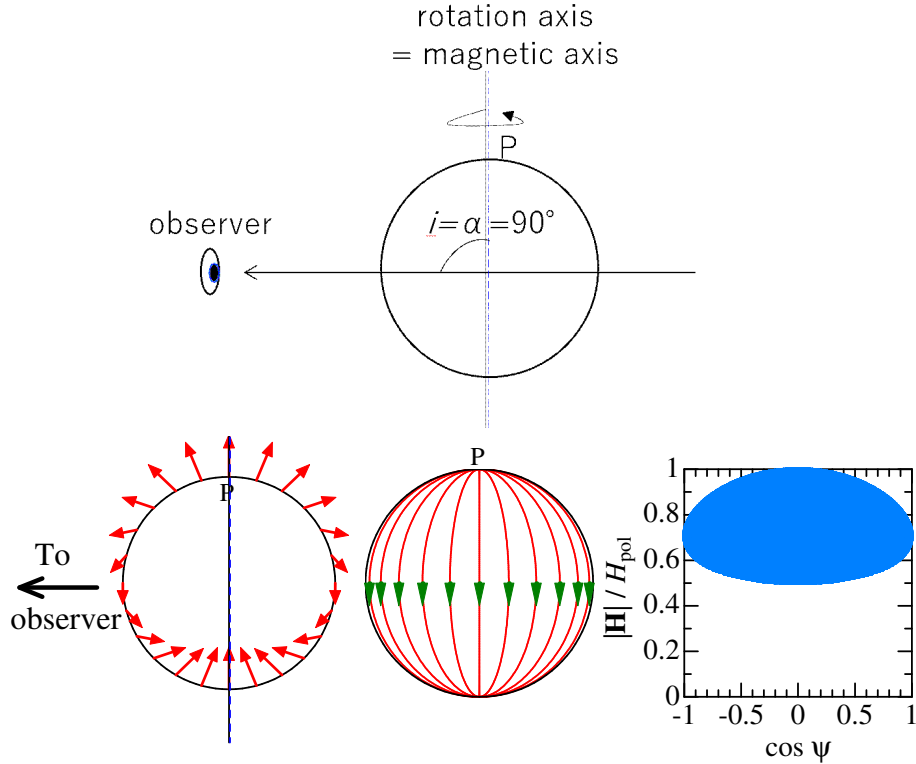


FIGURE 5 The upper figure schematically describes the adopted rotating star model with a dipole magnetic field (parameterized by H_{pol} ; field strength at the pole P), where the observer's line of sight is perpendicular to both of the rotational axis ($i = 90^\circ$) and the magnetic axis ($\alpha = 90^\circ$). The lower three figures represent the observed characteristics of the magnetic field in this model: Left — surface field vectors (indicated by arrows) in the meridional plane. Center — schematic illustration of surface magnetic field lines viewed by an observer. Right — Correlation between $|\mathbf{H}|/H_{\text{pol}}$ (absolute field strength in unit of H_{pol} and $\cos \psi$ (ψ is the angle between the magnetic field vector and the line of sight) at each point of the visible disk.

The resulting $\sigma_W(H_{\text{pol}}, v_t)$ values derived from Fe I and Fe II lines are given in Table 2, and the contours of σ_W on the $H_{\text{pol}}-v_t$ plane are depicted in Fig. 7. As seen from the locations of minimum σ_W , H_{pol} solutions for Fe I (~ 0 G) and Fe II (~ 2000 G) are rather conflicting, though $v_t \sim 1.5$ km s $^{-1}$ is consistently obtained irrespective of the species.

5.2 | Line widths analysis

Next, we extract information of magnetic field from the line width (h), where the contribution of $v_e \sin i$ plays an important role. For this purpose, the observed width (h_{obs}) is compared with the theoretical width ($h_{\text{cal}}^{7.8}$) calculated for various combinations of H_{pol} and $v_e \sin i$ but for fixed $A = 7.8$ and $v_t = 1.5$ km s $^{-1}$ (according to the result of Sect. 5.1). Similarly to Eq. (1), we define σ_h (function of H_{pol} and $v_e \sin i$) as

$$\sigma_h \equiv \sqrt{\sum_{n=1}^N (h_{v,\text{cal},n}^{7.8} - h_{v,\text{obs},n}^0)^2 / N}. \quad (4)$$

Here, $h_{v,\text{obs}}^0 \equiv \sqrt{h_{v,\text{obs}}^2 - 3^2}$ is the observed line width (in km s $^{-1}$) corrected for the instrumental effect (FWHM of 3 km s $^{-1}$), where the fact that line profiles are well approximated by Gaussian function (cf. Fig. 2e) was taken into account.

The resulting $\sigma_h(H_{\text{pol}}, v_e \sin i)$ values derived from Fe I and Fe II lines are given in Table 3, and the contours of σ_h on the $H_{\text{pol}}-v_e \sin i$ plane are depicted in Fig. 8. Inspecting the locations of minimum σ_h , we obtain $H_{\text{pol}} \sim 3000$ G and $v_e \sin i \sim 5$ km s $^{-1}$ for both Fe I and Fe II lines.

6 | DISCUSSION

6.1 | Results and their characteristics

In Sect. 5, we derived the magnetic field of *o* Peg (H_{pol} or $\langle H \rangle$) and the related line-broadening parameters (v_t and $v_e \sin i$) by comparing the observed and simulated equivalent widths (W) and line widths (h). The results are summarized in Table 4.

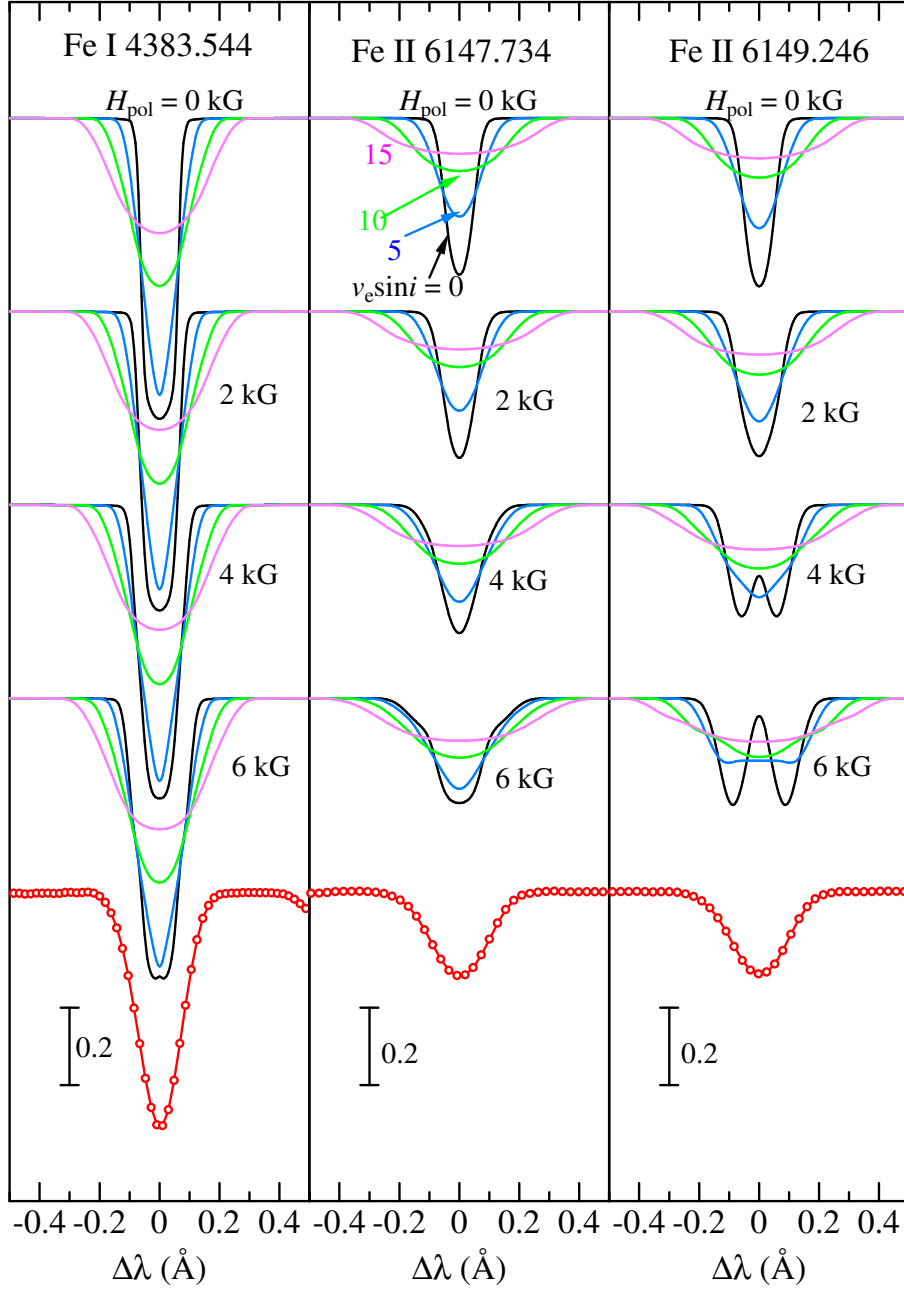


FIGURE 6 Demonstrative examples of theoretical flux profiles simulated by disk integration of unpolarized specific intensities (Stokes I) for three representative lines: Fe I 4383.544 (left), Fe II 6147.734 (center), and Fe II 6149.246 (right). Shown here are results calculated with $v_t = 1.5 \text{ km s}^{-1}$ for four H_{pol} values (0, 2, 4, and 6 kG) and four $v_e \sin i$ values (0, 5, 10, and 15 km s^{-1}). In addition, the actually observed profiles of $o \text{ Peg}$ are also displayed at the bottom for comparison. These simulated profiles of Fe II 6147.734 and 6149.246 may be compared with Fig. 2a and Fig. 2b of T91b, where the Zeeman-split structures are more manifest (because they are specific intensity profiles for single-valued magnetic field along with the assumption of $v_t = 0 \text{ km s}^{-1}$ without rotational broadening).

Since the velocity parameter solutions (η^{k^*} at the grid node $k = k^*$, where η denotes either v_t or $v_e \sin i$) have rounded values because the grids are rather coarse, σ was analytically expressed by a second-order polynomial of η by using

$\sigma(k^* - 1)$, $\sigma(k^*)$, and $\sigma(k^* + 1)$, from which the new η solution (η^{est}) was estimated as corresponding to the minimum of this parabolic $\sigma(\eta)$. Such derived v_t^{est} and $v_e \sin i^{\text{est}}$ are also given in Table 4.

TABLE 2 Calculated σ_W values as functions of H_{pol} and v_t .

v_t	$H_{\text{pol}} = 0$	500	1000	1500	2000	2500	3000	3500	4000	
	$\langle H \rangle = 0$	321	642	962	1283	1604	1925	2246	2566	
		(Fe I lines)								
3.0	9.004	9.037	9.128	9.274	9.471	9.711	9.985	10.285	10.607	
2.5	6.607	6.647	6.757	6.932	7.165	7.444	7.760	8.101	8.462	
2.0	4.445	4.491	4.614	4.810	5.068	5.376	5.721	6.091	6.476	
1.5	<u>3.164</u>	3.192	3.273	3.414	3.615	3.873	4.176	4.511	4.866	
1.0	<u>3.552</u>	3.530	3.483	3.438	3.428	3.473	3.581	3.748	3.961	
0.5	4.613	4.557	4.420	4.239	4.057	3.909	3.815	3.786	3.823	
0.0	5.105	5.037	4.870	4.647	4.411	4.199	4.036	3.935	3.901	
		(Fe II lines)								
3.0	13.143	13.239	13.500	13.914	14.463	15.129	15.892	16.734	17.642	
2.5	8.508	8.610	8.890	9.337	9.933	10.658	11.486	12.400	13.379	
2.0	5.097	5.163	5.357	5.707	6.226	6.903	7.714	8.631	9.629	
1.5	5.323	5.247	5.085	4.934	4.903	5.078	5.491	6.122	6.925	
1.0	8.094	7.933	7.543	7.021	<u>6.477</u>	6.017	5.740	5.717	5.973	
0.5	10.537	10.334	9.838	9.158	8.403	7.669	7.041	6.595	6.398	
0.0	11.481	11.261	10.730	10.001	9.186	8.376	7.655	7.095	6.759	

Given in this table are the values of σ_W [standard deviation between the observed and calculated equivalent widths in unit of mÅ; defined by Eq. (1)] calculated for each combination of H_{pol} (field strength at the magnetic pole in unit of G; see the top row) and v_t (microturbulence in unit of km s⁻¹; see the leftmost column). At the second row, the mean field strengths (in G) averaged over the stellar disk [$\langle H \rangle$; cf. Eq.(3)] corresponding to each H_{pol} are given. The minimum σ_W among each group is indicated by an underline.

TABLE 3 Calculated σ_h values as functions of H_{pol} and $v_e \sin i$.

$v_e \sin i$	$H_{\text{pol}} = 0$	500	1000	1500	2000	2500	3000	3500	4000	
	$\langle H \rangle = 0$	321	642	962	1283	1604	1925	2246	2566	
		(Fe I lines)								
15.0	14.936	14.946	14.977	15.029	15.100	15.191	15.303	15.438	15.597	
12.5	10.608	10.621	10.661	10.727	10.819	10.940	11.089	11.268	11.480	
10.0	6.343	6.361	6.414	6.503	6.628	6.792	6.997	7.243	7.532	
7.5	2.265	2.288	2.359	2.480	2.654	2.886	3.178	3.530	3.942	
5.0	2.116	2.082	1.988	1.841	1.661	1.491	1.405	1.485	1.762	
2.5	5.133	5.079	4.928	4.677	4.337	3.929	3.490	3.066	2.724	
0.0	6.127	6.073	5.916	5.645	5.263	4.793	4.274	3.751	3.280	
		(Fe II lines)								
15.0	13.736	13.749	13.789	13.853	13.940	14.050	14.184	14.344	14.532	
12.5	9.675	9.691	9.739	9.818	9.928	10.069	10.244	10.454	10.702	
10.0	5.684	5.705	5.767	5.871	6.017	6.207	6.445	6.732	7.071	
7.5	1.937	1.963	2.040	2.175	2.372	2.638	2.977	3.389	3.873	
5.0	2.149	2.109	1.999	1.829	1.631	1.466	1.442	1.645	2.063	
2.5	4.736	4.675	4.503	4.221	3.847	3.421	<u>3.005</u>	2.684	2.548	
0.0	5.588	5.525	5.344	5.034	4.611	4.120	3.629	3.207	2.923	

Given in this table are the values of σ_h [standard deviation between the observed and calculated full-width at half-maximum in unit of km s⁻¹; defined by Eq. (4)] calculated for each combination of H_{pol} (field strength at the magnetic pole in unit of G; see the top row) and $v_e \sin i$ (projected rotational velocity in unit of km s⁻¹; see the leftmost column). The minimum σ_h among each section is indicated by an underline. Otherwise, the same as in Table 2.

By inspecting these tables, we can read the following consequences regarding the magnetic field strength $\langle H \rangle$ (as well as v_t and $v_e \sin i$) of *o* Peg.

- Regarding the equivalent width analysis, contradicting results are obtained for $\langle H \rangle$ (~ 0 kG from Fe I lines and ~ 1.3 kG from Fe II lines). However, since the former is likely to be less reliable for the reason described in Sect. 3.3, we preferentially adopt the latter solution of

$\langle H \rangle \sim 1.3$ kG. Meanwhile, v_t is consistently settled at ~ 1.5 km s⁻¹.

- As to the line width analysis, mean field strengths of $\langle H \rangle \sim 1.9$ kG are derived for both Fe I and Fe II lines. The projected rotational velocity is concluded to be $v_e \sin i \sim 5$ km s⁻¹.
- Based on these results, although the $\langle H \rangle$ value from W tends to be somewhat lower than that from h , the mean

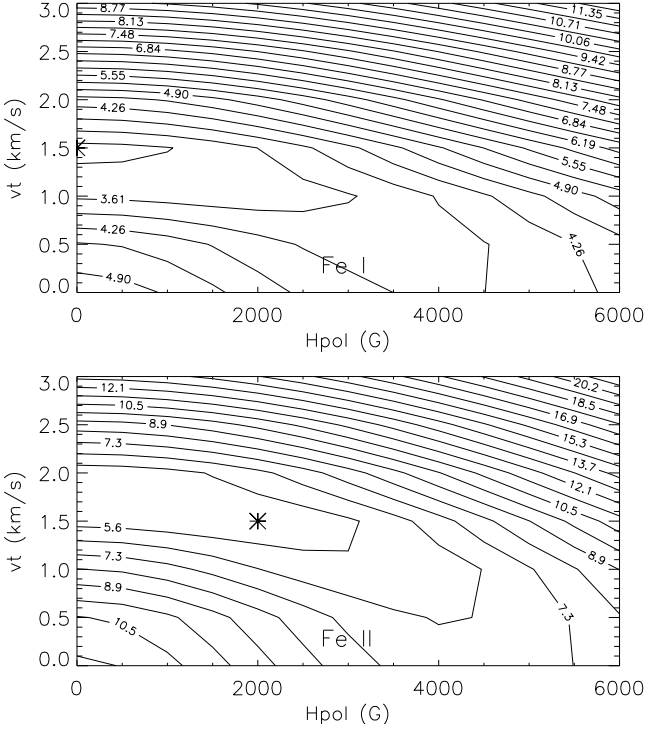


FIGURE 7 Graphical display of the contours of σ_W on the $H_{\text{pol}}-v_t$ plane, where the results for Fe I and Fe II lines are separately displayed in the upper and lower panels, respectively. In each panel, the position of $(H_{\text{pol}}^*, v_t^*)$ corresponding to the minimum σ_W is indicated by an asterisk (*).

magnetic field on the order of $\langle H \rangle \sim 1.5\text{--}2$ kG in *o* Peg is anyhow confirmed. Accordingly, the consequence of our new analysis is almost consistent with the conclusion of previous studies (ML90, T91b, T93), which reported the existence of $H \sim 2$ kG in this star.

- We may state that the impact of magnetic field is not very significant on the spectroscopic determination of v_t and $v_e \sin i$, because the resulting values (~ 1.5 km s⁻¹ and ~ 5 km s⁻¹) are not much different from those derived by neglecting the magnetic effect ($v_t \sim 1.7\text{--}1.8$ km s⁻¹ derived in Sect. 3.2, and the typical recent literature values of $v_e \sin i$ are $\sim 6\text{--}7$ km s⁻¹ as seen in Table 1). Regarding v_t , this is a reconfirmation of the argument in T93 (but not that in T91b).

6.2 | Precision check of T93 approximation

In the analysis of equivalent widths (Sect. 5.1), we could establish the magnetic field of *o* Peg from Fe II lines ($H_{\text{pol}} \sim 1.5\text{--}2$ kG), but not from Fe I lines (i.e., a well-defined minimum is not found in σ_W which continues to decline with a decrease in H_{pol} until $H_{\text{pol}} \rightarrow 0$). This situation is rather similar to the

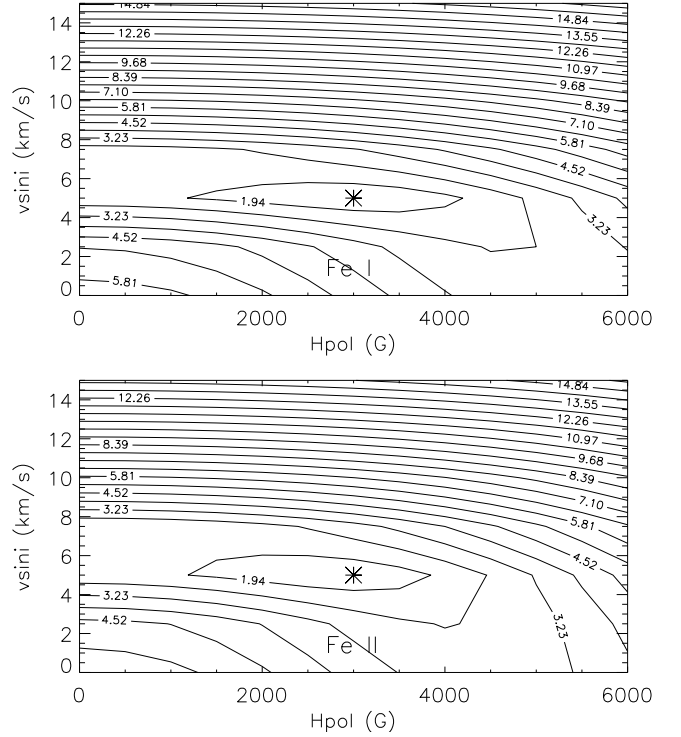


FIGURE 8 Graphical display of the contours of σ_h on the $H_{\text{pol}}-v_e \sin i$ plane, where the results for Fe I and Fe II lines are separately displayed in the upper and lower panels, respectively. In each panel, the position of $(H_{\text{pol}}^*, v_e \sin i^*)$ corresponding to the minimum σ_h is indicated by an asterisk (*).

case of T93, where a successful result was obtained from Fe II lines but not from Fe I lines (see the run of σ_b depicted in the middle-row panels of Fig. 2 in T93).

In T93, a practical (but approximate) method was used for evaluating the line flux equivalent width under the existence of magnetic field, in which the conventional spectrum-synthesis code is applicable without any necessity of solving the transfer equation of polarized radiation (cf. Sect. 2 in T93 for a detailed explanation). Briefly speaking, in this method, two equivalent widths are calculated for a given H corresponding to the minimum intensification (W_a ; using only σ_- and σ_+ components but independently from each other) and maximum intensification (W_c ; use of σ_- , σ_+ , and π components altogether while assuming as if no polarization effect exists). Then, it was assumed in T93 that the theoretical equivalent width to be adopted (which should be between W_a and W_c) is given by the “simple mean” of these minimum and maximum as $W_b(H) \equiv [W_a(H) + W_c(H)]/2$.

In order to examine the precision of this approximation, W_b values were calculated at various field strengths (H) for all of the 380 Fe lines (with $A = 7.8$ and $v_t = 1.5$ km s⁻¹),

TABLE 4 Summary of solutions based on line-strength or line-width analysis.

(Line strengths analysis)				
Species	H_{pol}^*	$\langle H \rangle^*$	v_t^*	v_t^{est}
Fe I	0	0	1.5	1.37
Fe II	2000	1283	1.5	1.52
(Line widths analysis)				
Species	H_{pol}^*	$\langle H \rangle^*$	$v_e \sin i^*$	$v_e \sin i^{\text{est}}$
Fe I	3000	1925	5.0	5.10
Fe II	3000	1925	5.0	5.01

Quantities with asterisks (*) in column 2–4 are the solutions corresponding to the minimum of σ_W or σ_h , while that in column 5 is the estimated solution derived by quadratic interpolation (see Sect. 6.1).

which were then compared with the corresponding W_{cal} values simulated in Sect. 4.3.

The resulting W vs. H relations (based on different methods of T93 and this study) for three representative lines (Fe I 4383.544, Fe II 6147.734, and Fe II 6149.246) are compared in Figs. 9a, 9b, and 9c, respectively. We can see from these figures that $W_b(H)$ (solid line) is a reasonable approximation of $W_{\text{cal}}(\langle H \rangle)$ (symbols), though some systematic departure is observed at larger H depending on lines.⁶ The logarithmic differences between W_b and W_{cal} for all lines are plotted against W_{cal} in Figs. 9d, 9e, and 9f for different field strengths of 0, 2, and 4 kG, respectively. These figures indicate that $|\log(W_b/W_{\text{cal}})|$ is typically a few hundredths dex at most (i.e., several or $\lesssim 10$ percent in W) even at the magnetic field of 4 kG. Accordingly, the practical approach proposed by T93 for calculating equivalent widths of a magnetic star may be regarded as a reasonable approximation of moderate precision (especially when the lines to be used are carefully chosen).

6.3 | Implication from the line-pair method

Finally, as an application of the simulations done in Sect. 4, we estimate the magnetic field of σ Peg based on the very simple approach using the strengths of specific line pairs belonging to the same multiplet, which was first tried by ML90 and then

extended by T91b. This method makes use of the relative difference of equivalent widths for the two lines (1 and 2) defined as $\delta \equiv 2(W_1 - W_2)/(W_1 + W_2)$. While $\delta \simeq 0$ in the non-magnetic case, δ begins to depart from zero with an increase in H (because of the different H -sensitivity between lines 1 and 2). Accordingly, H may be estimated by comparing the observed δ_{obs} with the known δ vs. H relation.

Here, two line pairs are relevant, which are called after T91b as “red pair (R)” (Fe II 6147.7 and 6149.2) and “blue pair (B)” (Fe II 4416.8 and 4385.4). See Table 1 of T91b for more details on these line pairs. Since these 4 Fe II lines are included in our 380 target lines, δ_R and δ_B at various field strengths can be evaluated from their W_{cal} results⁷ calculated at $H_{\text{pol}} = 0, 500, 1000, \dots, 5500,$ and 6000 G (along with $v_t = 1.5 \text{ km s}^{-1}$ and $A = 7.8$).

The resulting theoretical δ_R and δ_B are plotted against $\langle H \rangle$ in Fig. 10, where the positions of $\delta_R = +0.025$ and $\delta_B = -0.020$ derived from the observed equivalent widths in mÅ ($W_{1,R}/W_{2,R} = 49.8/48.6$, $W_{1,B}/W_{2,B} = 91.5/93.4$) are also indicated. The following trends can be read from this figure.

- A comparison of theoretical and observed δ_R yields a mean magnetic field strength of $\langle H \rangle \sim 2.4$ kG.
- Regarding δ_B , a unique solution can not be found. What can be said from Fig. 10 is that $\langle H \rangle$ is either ~ 1.3 kG or ~ 2.9 kG.
- In any case, these results do not contradict the consequence of the main analysis (detection of $\langle H \rangle$ on the order of ~ 2 kG; cf. Sect. 6.1).

6.4 | Magnetic nature of σ Peg

Our analysis on the line strengths and widths has thus corroborated that an appreciable magnetic field of $\langle H \rangle \sim 1\text{--}2$ kG (mean field strength averaged over the disk) exists in the Am star σ Peg. Here, we should recall that previous spectropolarimetric observations conducted so far failed to detect any meaningful signal of circular polarization in this star (cf. Sect. 1), which means that $\langle H_z \rangle$ (mean line-of-sight component of the field averaged over the disk) is very weak. Although detection of ultra-weak $\langle H_z \rangle$ on the order of several G might as well be possible by using higher-precision observations (see footnote 1), we can at least state that $\langle H_z \rangle$ is negligibly weak compared to $\langle H \rangle$.

One possibility to explain this marked disagreement is that the magnetic field is not globally organized but has a complex structure (such as suggested by ML90). If several or more strong magnetic regions of smaller scale with different polarities exist on the stellar disk (such as sunspots), the net

⁶We may state that a line with single (or practically single) σ_- or σ_+ component (such like the cases of Fe I 4383.544 or Fe II 6149.246) tends to suffer an appreciable deviation, since the difference between W_a and W_c is comparatively large because W_a is H -independent and constant (cf. Figs. 9a and 9c). In contrast, if σ_- (or σ_+) components of a line are sufficiently apart (like Fe II 6147.734), W_b makes a fairly good approximation for W_{cal} , because W_a and W_c increase with H in somewhat similar manner and the difference tends to be small (cf. Fig. 9b).

⁷Since the $\log gf$ values of the lines consisting the pair given in the VALD database (which we adopted in this study) are rather discrepant from each other, the requirement of $\delta \simeq 0$ in the non-magnetic case is not fulfilled if $\log gf$ (VALD) data were used. Therefore, the $\log gf$ values presented in Table 1 of T91b were exceptionally employed here for both of the red-pair lines and blue-pair lines.

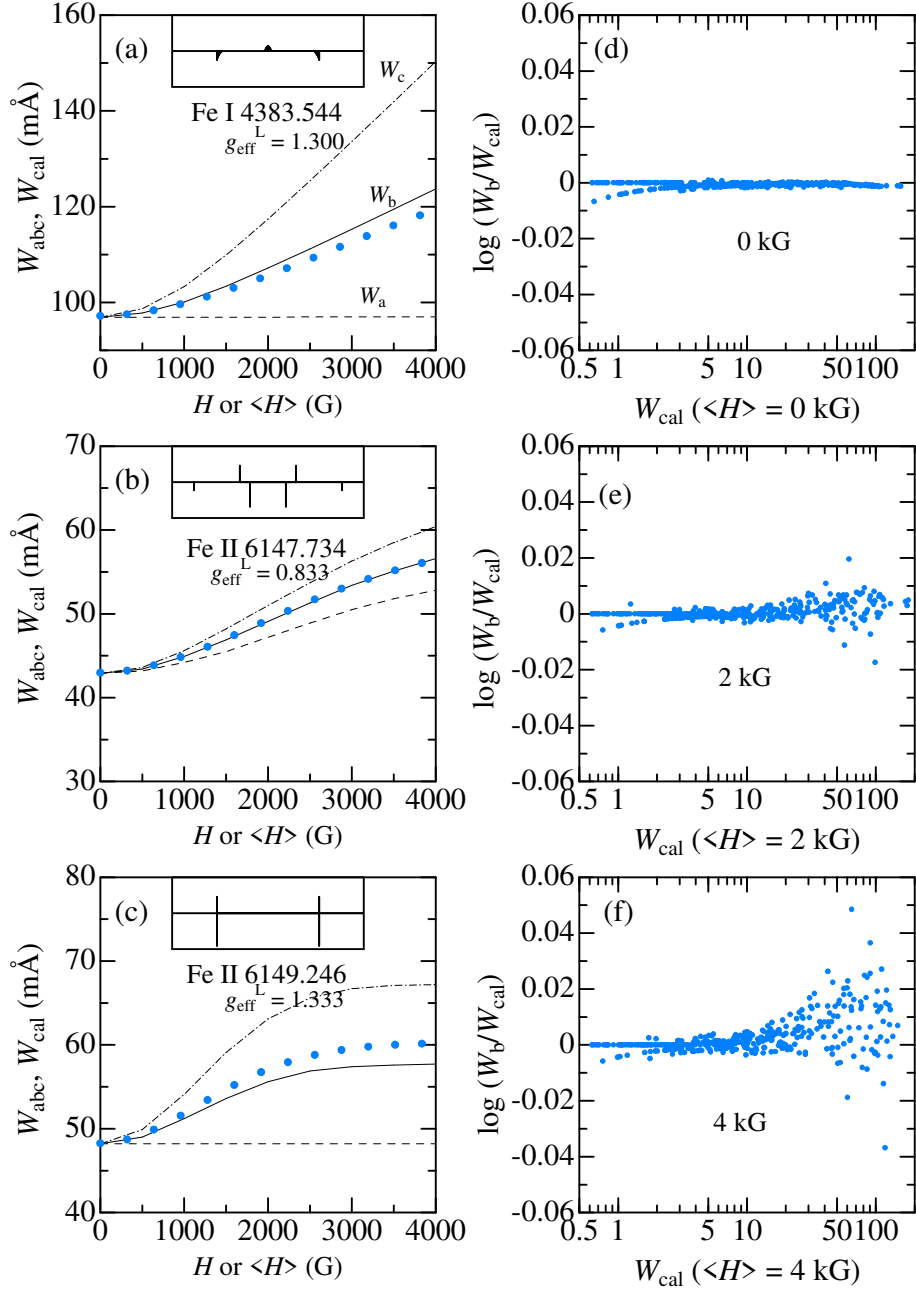


FIGURE 9 Left panels (a–c) show how the flux equivalent width varies by changing the magnetic field strength for three representative lines: (a) Fe I 4383.544, (b) Fe II 6147.734, and (c) Fe II 6149.246 (their Zeeman patterns are shown in the inset of each panel). Those evaluated by the WIDTH9 program with three kinds of approximations proposed in T93, W_a (minimum intensification involving only σ_- and σ_+ components), W_c (maximum intensification for the case of neglecting the polarization effect), and W_b (simple mean of W_a and W_c ; finally adopted in T93), are depicted in dashed line, dash-dotted line, and solid line, respectively. Meanwhile, those calculated based on our dipole magnetic field model by disk integration of local I profiles (W_{cal}) are plotted by filled symbols. Note that these W_{cal} values are plotted against $\langle H \rangle$ (not H_{pol}). All these W calculations were done with $A = 7.80$ and $v_t = 1.5 \text{ km s}^{-1}$. The logarithmic differences evaluated for all 380 Fe lines [$\log(W_b/W_{cal})$] are plotted against W_{cal} in the right panels (d–f) for different mean field strengths ($\langle H \rangle$): (d) 0 kG, (e) 2 kG, and (f) 4 kG.

line-of-sight component of the field ($\langle H_z \rangle$) would almost vanish while the mean magnetic field strength ($\langle H \rangle$) still remains

detectable. However, it seems that very strong magnetic spots or patches (with strengths considerably exceeding ~ 2 kG) are

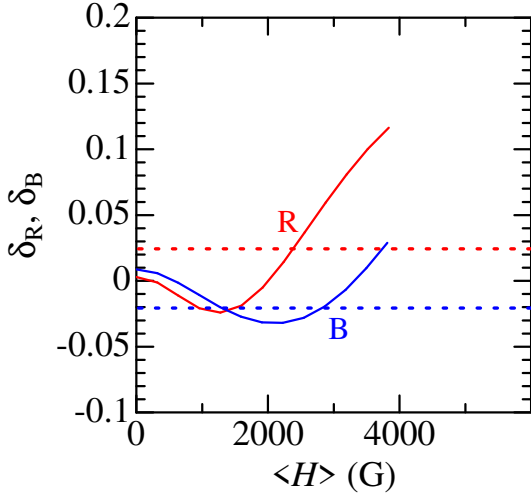


FIGURE 10 Relative differences of equivalent widths [$\delta \equiv 2(W_1 - W_2)/(W_1 + W_2)$] for the red (R) and blue (B) pair lines (cf. Table 1 in T91b) are plotted against the mean field strength ($\langle H \rangle$) by solid lines, which were calculated with $A = 7.80$ and $v_t = 1.5 \text{ km s}^{-1}$. The observed values ($\delta_R = +0.025$, $\delta_B = -0.020$) are indicated by horizontal dotted lines.

rather unlikely in the present case, because they should give rise to some kind of appreciable peculiarities in the profiles of magnetically-sensitive lines. For example, if assumed that 1/3 of the stellar disk is covered by a strong magnetic patch of $H \sim 6 \text{ kG}$ while the remaining 2/3 is non-magnetic, Fe II 6149.246 line would show a complex profile as expected from the simulation; but such an anomalous feature is absent in the actual profile which is nearly Gaussian (cf. the right panel of Fig. 6).

Accordingly, whichever configuration of the magnetic field, the field contrast over the stellar disk would not be distinctly large (i.e., not so much like spots/patches as rather gradual). In this context, the simple rotating dipole model of aligned rotational/magnetic axis viewed almost equator-on ($i \simeq \alpha \simeq 90^\circ$), which was assumed in the simulation of this study, may be regarded as the likely solution for *o* Peg, because it naturally explains the observational fact of $\langle H_z \rangle \sim 0$. Although it is not easy to check this hypothesis observationally, some weak rotational modulation of circular polarization might as well be detected if α is not exactly (but slightly deviates from) 90° . In this case, the rotation period is estimated as $P \simeq 42 \text{ d}$ by combining $v_e (\simeq v_e \sin i) \simeq 5 \text{ km s}^{-1}$ and $R \simeq 4.4R_\odot$. It may thus be worthwhile to examine whether a modulation period of $\sim 40 \text{ d}$ is observed for this star by ultra high-precision spectropolarimetry.

7 | SUMMARY AND CONCLUSION

The star *o* Peg is a representative A-type star (classified as a hot Am star from its abundance characteristics), which has been frequently studied by a number of investigators because of its brightness and sharp-line nature.

In the early 1990s, several authors (ML90, T91b, T93) reported the existence of surface magnetic field on the order of $\sim 2 \text{ kG}$ in this star based on the analysis of widths or strengths of many spectral lines, which was a significant finding because the conventional spectropolarimetry has been unsuccessful in detecting any meaningful signal of $\langle H_z \rangle$.

However, the techniques employed by these old studies were not necessarily founded on a physically legitimate basis but rather empirical or approximate in character. Besides, the quality of the adopted spectra of *o* Peg, on which the observational data of line widths and strengths were measured, was not satisfactory as viewed from the present-day standard.

Given that this detection does not seem to have been corroborated since then, I decided to revisit this issue based on (i) an improved modeling of theoretical line flux profile of a rotating magnetic star (by disk integration of local intensity profiles obtained by correctly solving the transfer equation of polarized radiation) and (ii) using the high-resolution ($R \sim 100000$) and very high S/N (~ 1000) spectra of *o* Peg.

The magnetic and rotational axes of this model star (with a dipole field) were assumed to be in line with each other and perpendicular to the observer's line of sight ($i = \alpha = 90^\circ$), by which $\langle H_z \rangle = 0$ is attained in accordance with observations.

As for the spectral lines whose full-widths at half-maximum (h) and equivalent widths (W) are to be analyzed, 380 Fe lines (198 Fe I and 182 Fe II lines) were carefully selected, which are free from any serious blending effect.

The conventional analysis (without taking into account the effect of magnetic intensification) of equivalent widths was first carried out, which resulted in $A \simeq 7.8$ (Fe abundance) and $v_t \simeq 1.7\text{--}1.8 \text{ km s}^{-1}$ (microturbulence). This result of $A(\text{Fe}) = 7.8$ was used as the fiducial abundance to be fixed throughout the subsequent magnetic field analyses.

By requiring the minimum dispersion between the theoretical W values simulated with the magnetic field model (depending on the field strength and microturbulence) and the observed ones, we found that $\langle H \rangle \sim 1.3 \text{ kG}$ (from Fe II lines) and $v_t \sim 1.5 \text{ km s}^{-1}$.

Similarly, by comparing the simulated h values (function of projected rotational velocity and magnetic field strength) with the measured ones, the best solutions accomplishing the least dispersion were derived as $\langle H \rangle \sim 1.9 \text{ kG}$ and $v_e \sin i \sim 5 \text{ km s}^{-1}$.

Based on these results, although the $\langle H \rangle$ value from the analysis of W tends to be somewhat lower than that from h ,

the mean magnetic field on the order of $\langle H \rangle \sim 1\text{--}2$ kG has been confirmed in α Peg.

In addition, supplementary applications of the simulated W results were also conducted for checking purposes: (i) The precision of the practical method proposed by T93 for evaluating W in the presence of a magnetic field was examined and confirmed to be a reasonable and useful approximation. (ii) The line-pair method used by ML90 and T91b was applied based on the newly simulated W values of specific line pairs and found that H is in the range of $\sim 1\text{--}3$ kG.

In summary, the consequence resulting from our analysis on the W and h data of Fe lines is almost consistent with the conclusion of previous studies (ML90, T91b, T93) which reported $H \sim 2$ kG for this star.

Regarding the reason for the marked discrepancy between $\langle H \rangle \sim (1\text{--}2$ kG) and $\langle H_z \rangle (\sim 0)$, an accidental accomplishment of $i \simeq \alpha \simeq 90^\circ$ in the poloidal configuration might as well be ponderable, rather than invoking a complex structure with small-scale magnetic regions of different polarities.

ACKNOWLEDGMENTS

This research has made use of the SIMBAD database, operated by CDS, Strasbourg, France. This work has also made use of the VALD database, operated at Uppsala University, the Institute of Astronomy RAS in Moscow, and the University of Vienna.

DATA AVAILABILITY

The basic data and results underlying this article are presented as the online supplementary material. The line profile data used for measurements are given in “obsprofiles.dat”, while the original spectra of α Peg are in the public domain and available at <https://smoka.nao.ac.jp/index.jsp> (SMOKA Science Archive site).

SUPPORTING INFORMATION

This article accompanies the following online materials.

- [ReadMe.txt](#)
- [felines.dat](#)
- [obsprofiles.dat](#)

REFERENCES

Abt, H. A., & Morrell, N. I., 1995, *ApJS*, 99, 135.

- Adelman, S. J., 1973, *ApJ*, 183, 95.
 Adelman, S. J., 1988, *MNRAS*, 230, 671.
 Adelman, S. J., & Fuhr, J. R., 1985, *A&A*, 152, 434.
 Adelman, S. J., Cowley, C. R., & Hill, G., 1988, in *Elemental Abundance Analyses*, ed. S. J., Adelman & T. Lanz (Lausanne: Institut de l'Université de Lausanne), p.15.
 Adelman, S. J., Pintado, O. I., Nieva, F., Rayle, K. E., & Sanders, S. E., Jr., 2002, *A&A*, 392, 1031.
 Adelman, S. J., Young, J. M., & Baldwin, H. E., 1984, *MNRAS*, 206, 649.
 Allen, M. S., 1977, *ApJ*, 213, 121.
 Babcock, H. W. 1958, *ApJ*, 128, 228.
 Blackwell, D. E., Ibbetson, P. A., Petford, A. D., & Willis, R. B., 1976, *MNRAS*, 177, 227.
 Blackwell, D. E., & Lynas-Gray, A. E., 1998, *A&AS*, 129, 505.
 Blazère, A., et al., 2016a, *A&A*, 586, A97.
 Blazère, A., Neiner, C., & Petit, P., 2016b, *MNRAS*, 459, L81.
 Blazère, A., Petit, P., Neiner, C., Folsom, C., Kochukhov, O., Mathis, S., Deal, M., & Landstreet, J., 2020, *MNRAS*, 492, 5794.
 Burkhardt, C., & Coupry, M. F., 1991, *A&A*, 249, 205.
 Bychkov, V. D., Bychkova, L. V., & Madej, J., 2009, *MNRAS*, 394, 1338.
 Castelli, F., & Hack, M., 1988, in *Elemental Abundance Analyses*, ed. S. J., Adelman & T. Lanz (Lausanne: Institut de l'Université de Lausanne), p.23.
 Conti, P. S., & Strom, S. E., 1968, *ApJ*, 154, 975.
 Di Benedetto, G. P., 1998, *A&A*, 339, 858.
 Gray, D. F., 2014, *AJ*, 147, 81.
 Hensberge, H., & De Loore, C., 1974, *A&A*, 37, 367.
 Hill, G. M., 1995, *A&A*, 294, 536.
 Hill, G. M., & Landstreet, J. D., 1993, *A&A*, 276, 142.
 Hui-Bon-Hoa, A., 2000, *A&AS*, 144, 203.
 Kocer, D., Bolcal, Ç., & Saatici, M. S., 1988, in *Elemental Abundance Analyses*, ed. S. J., Adelman & T. Lanz (Lausanne: Institut de l'Université de Lausanne), p.38.
 Kurucz, R. L., 1993, *Kurucz CD-ROM, No. 13* (Harvard-Smithsonian Center for Astrophysics).
 Landstreet, J. D., Kupka, F., Ford, H. A., Officer, T., Sigut, T. A. A., Silaj, J., Strasser, S., & Townshend, A., 2009, *A&A*, 503, 973.
 Mathys, G., 1990, *A&A*, 232, 151.
 Mathys, G., & Lanz, T., 1990, *A&A*, 230, L21 (ML90).
 Mitton, J., 1977, *A&AS*, 27, 35.
 Petit, P., et al., 2009, *A&A*, 532, L13.
 Prugniel, Ph., Vauglin, I., & Koleva, M., 2011, *A&A*, 531, A165.
 Renson, P., & Manfroid, J., 2009, *A&A*, 498, 961.
 Royer, F., Grenier, S., Baylac, M.-O., Gómez, A. E., & Zorec, J., 2002, *A&A*, 393, 897.
 Royer, F., Zorec, J., & Gómez, A. E., 2007, *A&A*, 463, 671.
 Ryabchikova, T., Piskunov, N., Kurucz, R. L., Stempels, H. C., Heiter, U., Pakhomov, Yu., & Barklem, P. S., 2015, *Phys. Scr.*, 90, 054005.
 Sadakane, K., 1988, in *Elemental Abundance Analyses*, ed. S. J., Adelman & T. Lanz (Lausanne: Institut de l'Université de Lausanne), p.42.
 Shorlin, S. L. S., Wade, G. A., Donati, J.-F., Landstreet, J. D., Petit, P., Sigut, T. A. A., & Strasser, S., 2002, *A&A*, 392, 637.
 Sokolov, N. A., 1995, *A&AS*, 110, 553.
 Stenflo, J. O., & Lindegren, L., 1977, *A&A*, 59, 367.
 Takeda, Y., 1991a, *PASJ*, 43, 719.
 Takeda, Y., 1991b, *PASJ*, 43, 823 (T91b).
 Takeda, Y., 1993, *PASJ*, 45, 453 (T93).
 Takeda, Y., 2020, *MNRAS*, 499, 1126.
 Takeda, Y., Kang, D.-I., Han, I., Lee, B.-C., Kim, K.-M., Kawanomoto, S., & Ohishi, N., 2012, *PASJ*, 64, 38.
 Takeda, Y., Kawanomoto, S., & Ohishi, 2008, *ApJ*, 678, 446.

- Takeda, Y., Kawanomoto, S., Ohishi, N., Kang, D.-I., Lee, B.-C., Kim, K.-M., & Han, I., 2018, *PASJ*, 70, 91.
- Unno, W., 1956, *PASJ*, 8, 108.
- Van't Veer, C., Coupry, M. F., & Burkhart, C., 1988, in *Elemental Abundance Analyses*, ed. S. J., Adelman & T. Lanz (Lausanne: Institut de l'Université de Lausanne), p.48.
- Wolff, S. C., 1967, *ApJS*, 15, 21.
- Zorec, J., Cidale, L., Arias, M. L., Frémat, Y., Muratore, M. F., Torres, A. F., & Martayan, C., 2009, *A&A*, 501, 297.
- Zorec, J., & Royer, F., 2012, *A&A*, 537, A120.

